ISSN 1063-780X, Plasma Physics Reports, 2023, Vol. 49, No. 10, pp. 1169–1179. © Pleiades Publishing, Ltd., 2023.
Russian Text © The Author(s), 2023, published in Fizika Plazmy, 2023, Vol. 49, No. 10, pp. 964–974.

ION AND PLASMA SOURCES

Comparative Analysis of High-Frequency Plasma Drivers with Various Protective Screens for Atomic Injectors with Multi-Second Pulse Duration

D. Yu. Gavrisenko[a,*], I. V. Shikhovtsev[a], Yu. I. Belchenko[a], A. I. Gorbovskiy[a], A. A. Kondakov[a], O. Z. Sotnikov[a], A. L. Sanin[a], V. A. Vointsev[a], and R. A. Finashin[a]

[a] *Budker Institute of Nuclear Physics, Siberian Branch, Russian Academy of Sciences, Novosibirsk, 630090 Russia*

**e-mail: d.gavrisenko@g.nsu.ru*

Received May 18, 2023; revised July 17, 2023; accepted July 20, 2023

Abstract—Atomic beam injection is one of the main methods of plasma heating in thermonuclear facilities. An injector of high-energy hydrogen atoms for plasma heating based on the acceleration and neutralization of negative hydrogen ions is being developed at the Budker Institute of Nuclear Physics, Siberian Branch of the Russian Academy of Sciences. The injector uses a surface plasma source, in which a plasma flow is created using a radio-frequency driver: an induction radio-frequency (RF) discharge, ignited inside a cylindrical ceramic chamber when an RF voltage is applied to an external antenna. As a part of this work, a new version of the RF driver is being developed. A protective screen is used to prevent overheating and erosion of the ceramic wall of the driver. The operation of RF driver with different protective screens is studied. These screens reduce the efficiency of RF power transmission into the discharge, but make it possible the operation of the ion source in multi-second or steady-state pulses.

Keywords: atomic beams, negative hydrogen ions, high-frequency driver, RF antenna, protective screen, ion source, multi-second pulse duration

DOI: 10.1134/S1063780X2360069X

1. INTRODUCTION

Neutral beam injectors are widely used in large fusion facilities for plasma heating and diagnostics. Injectors developed at the Budker Institute of Nuclear Physics, Siberian Branch, Russian Academy of Sciences (BINP) are successfully used in various facilities with magnetic plasma confinement [1, 2]. High-energy atomic beams are obtained as a result of the acceleration of positive or negative ions and their subsequent neutralization in a special target. Modern thermonuclear facilities require powerful injectors capable of working with beams lasting more than ten seconds.

One of the main elements of the injector is an ion source. To generate an ion source plasma, the radio-frequency (RF) drivers based on an inductive discharge in a ceramic chamber excited by an external antenna are generally used [2]. Such RF ion sources successfully operate in atomic beam injectors with multisecond pulse durations [3–7]. To increase the pulse duration of the plasma generator, a special protective screen is installed inside the RF driver, which protects ceramics from plasma erosion and metal sputtering. However, the protective screen reduces the plasma generation efficiency and the performance of the ion source. The problem of increasing the plasma generation efficiency in the RF driver is studied in the several research centers [8–10].

An RF surface-plasma source of negative hydrogen ions with a beam current of up to 1.5 A and an energy of up to 120 keV with a pulse duration of up to 20 s is being under development at the BINP within the work on a prototype high-energy atomic injector with a beam energy of up to 500 keV. To ensure the required negative ion beam current, the flux density of positive ions in the plasma at the output of the RF driver of 200 mm in diameter should be of about ~400 mA/cm^2.

The purpose of this work is to analyze and compare the efficiency of RF drivers with various protective screens and RF antennas.

2. EXPERIMENTAL STAND

The characteristics of various RF drivers were studied and their parameters were measured on an experimental stand shown in Fig. 1. It consists of a cylindrical vacuum volume (*5* in Fig. 1), to the end flange of which the RF driver under study is attached (*2* in Fig. 1). The stand is evacuated by a turbomolecular pump and is equipped with a hydrogen supply system

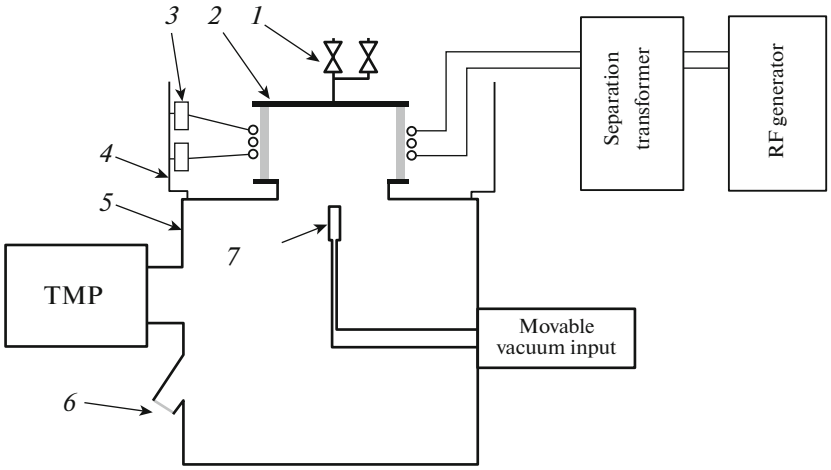

Fig. 1. Scheme of the experimental stand: (*1*) gas supply system with two valves, (*2*) RF driver, (*3*) resonant contour capacitors, (*4*) external cylindrical electrostatic screen, (*5*) vacuum volume, (*6*) window, (*7*) grid probe.

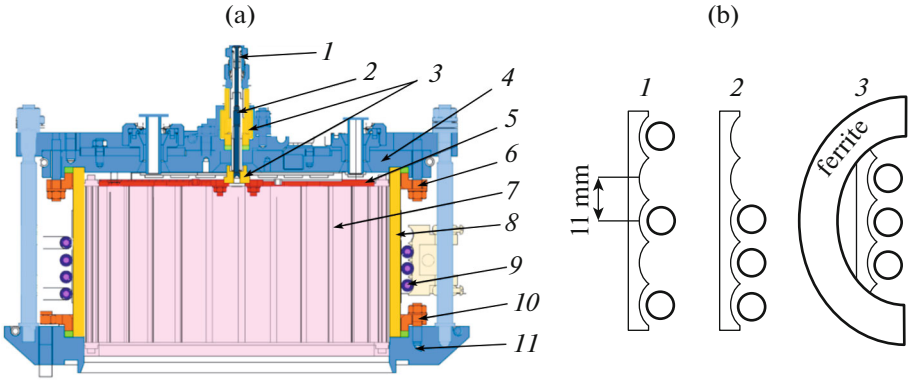

Fig. 2. (a) RF driver scheme: (*1*) hydrogen dispenser, (*2*) hydrogen inlet channel, (*3*) ignition unit insulators, (*4*) back flange, (*5*) back flange screen, (*6*) upper sealing ring, (*7*) protective screen, (*8*) Al_2O_3 ceramics chamber, (*9*) three-turn antenna, (*10*) lower sealing ring, (*11*) front flange, (b) three configurations of an external antenna: (*1*) stretched, (*2*) compressed and moved to the front flange, (*3*) compressed with ferrites.

(*1* in Fig. 1), a powerful RF power supply system and the necessary set of diagnostics (*7* in Fig. 1).

Basic Design of Radio-Frequency Plasma Driver

A scheme of an RF driver is shown in Fig. 2a. The driver chamber is a ceramic cylinder (Al_2O_3) with an internal diameter of 200 mm, a length of 111 mm and a wall thickness of 7 mm, clamped at the ends by back and front flanges. Ceramics is sealed at the edges of the outer cylindrical surface using Viton rings. clamped by steel rings (Fig. 2a-*6* and Fig. 2a-*10*). Thin copper foils are placed between the ceramic cylinder and the flanges (Fig. 2a-*4* and Fig. 2a-*11*) to improve the ceramics cooling.

A 3-turn antenna is wound around the ceramic cylinder outside to produce an RF electromagnetic field inside the volume. The antenna is made of a copper tube with a diameter of 6 mm, covered by dielectric heat-shrinkable shell. To cool the antenna, distilled water flows through it. The antenna is fixed outside of the ceramic cylinder with the different distance between the turns and the position of the antenna. Three variants of the tested antenna configurations are shown in Fig. 2b. Several antenna configurations were studied in the experiments: wide (Fig. 2b-*1*), low (Fig. 2b-*2*), narrow without ferrites, and narrow with ferrites (Fig. 2b-*3*). Ferrite half rings are made of M200VNP-3 K65 × 40 × 9 cores cut in half. Sixteen such half-rings were installed evenly in azimuth outside the antenna.

An ignition unit is installed in the center of the upper flange, which is necessary to produce initial electrons that initiate ignition of the RF discharge. It has a gas inlet channel with an electrically insulated electrode in the center. To supply gas, two electromagnetic valves with different diaphragms were used, an ignition valve to create conditions for ignition of the discharge and a working valve to maintain the discharge.

Permanent magnets, which create a multipole magnetic field structure near the back wall, are located on the back flange. The magnetic field helps to increase the discharge efficiency and reduce the plasma flow to the back wall.

For the RF driver to operate in modes with high power and pulse duration, its main components (protective screen, antenna, ignition unit, end flanges) are cooled by pumping distilled water. The remaining elements are cooled as a result of heat removal through the clamping contacts and from the outside by air convection. The main sources of heating of the RF driver elements are plasma flows onto the walls, ohmic losses in the RF antenna and eddy currents excited by the RF field in the protective screen, end and sealing flanges.

The driver operation scenario is as follows. First, hydrogen gas is supplied into the chamber through the ignition valve. This produces a pressure of about 1–2 Pa necessary to ignite the discharge. Then RF voltage is applied to the antenna, and a short (several microseconds) pulse with a voltage of about 3 kV is applied to the rod of the ignition unit. A spark is generated along the inner surface of the ceramic ignition insulator, the plasma of which enters the plasma chamber and ignites the RF discharge. After the discharge is ignited, the ignition valve closes and the operating valve opens, which maintains the required reduced hydrogen pressure of 0.3–0.6 Pa during the action of the high-frequency pulse.

Protective Screen Options

For long-duration pulses, a slotted protective screen is installed inside the ceramic chamber of the RF driver. This helps reduce the thermal load on the ceramics, prevent fast plasma particles from sputtering ceramics, and reduce metal sputtering. Longitudinal slots in the screen allow the RF field to penetrate inside the gas-discharge chamber. Protective screens can be divided by the type of cooling they have. A passively cooled screen transfers heat through mechanical contact of the screen with flanges or other cooled elements [1]. To actively cool the protective screen, cooling channels are made in it with outputs for supplying distilled water passing through the back flange of the RF driver.

The thin screen consists of molybdenum plates 1 mm thick, attached to cooled copper rings at the ends. Distillate is supplied to the cooling channels of the rings through tubes passing through the back flange of the RF driver. The connection of the plates to the rings is ensured by screws. The gaps between the screen plates make up 20% of the area of the inner surface of the screen.

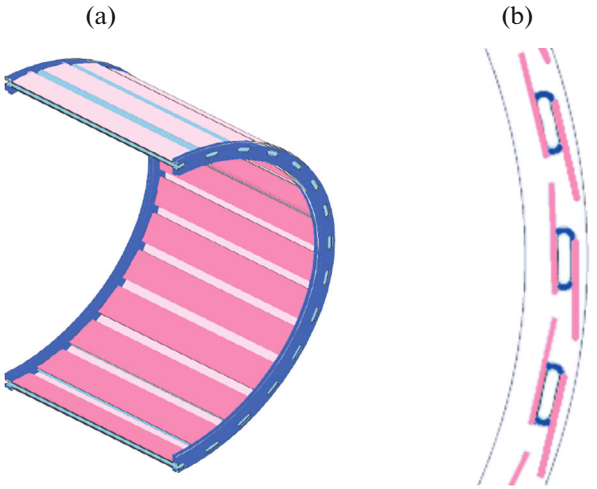

Fig. 3. Molybdenum screen with z-shaped slots. (a) 3D diagram of the screen, (b) cross section of the screen.

The soldered screen consists of two stainless rings and Z-shaped lamellas: stainless tubes with a diameter of 6 mm, flattened to a thickness of 4 mm with two soldered molybdenum plates 0.5 mm thick. The screen scheme is shown in Fig. 3. The distance between adjacent plates is 4.5 mm. The tubes are welded into manifolds with a diameter of 6 mm. The cooling channel forms an S turn passing through the blinds. The screen has two channels for each half, with outputs through the back flange of the RF driver. The total thickness of the side wall of the screen is 5 mm.

The molded slot screen is a copper screen with Z-shaped slots and internal cooling channels. It is developed at the Institute of Plasma Physics (Hefei, China) [10] and manufactured by diffusion welding at a Chinese enterprise (Hefei Keye Electrical Physical Equipment Manufacturing, China). The total thickness of the side wall of the screen is 6 mm.

Schemes for Connecting the RF Voltage to the Antenna

Figure 4 shows the equivalent scheme for supplying voltage to the antenna. A voltage of 3–9 kV and a frequency $f \approx 4$ MHz is supplied from a generator based on a powerful Eimac 4CW50000E tetrode through an isolation transformer to the RF driver antenna with a transmission ratio of 1 : 1. When directly connecting the antenna to such a transformer, it is impossible to obtain optimal matching of the generator with the

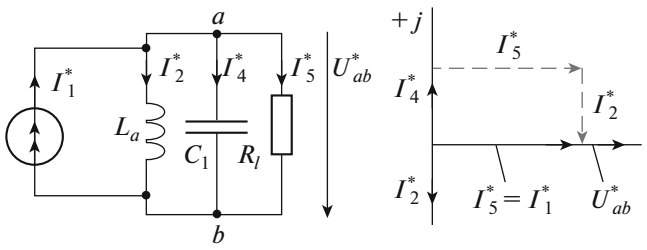

Fig. 4. Connection scheme of the RF generator to the resonant contour of the RF driver. Vector diagrams of currents and voltages at parallel resonance are given on the right.

load, which is the RF driver with plasma. Also, for the driver to operate efficiently, it is necessary to obtain a voltage at the antenna higher than the voltage at the anode of the RF generator lamp.

To increase the total voltage on the antenna, the RF generator was connected according to a scheme known in radio engineering as a circuit of the second type or an inductive three-point circuit. To implement the circuit, two taps were made on the antenna, to which the generator was connected. A matching option with partial inclusion of the antenna coil is shown in Fig. 5. In the implemented connection circuit described in more detail in [11], a higher voltage is generated at the ends of the antenna than that supplied from the generator due to the effects of resonant amplification. Vector diagrams explaining the operation of the antenna at resonance are shown in Fig. 5. For the given diagrams in Figs. 4 and 5: L_a, C_1, R_l are inductance, capacitance and resistive loads, and I_1, I_2, ..., I_n are currents in branches.

After analyzing the circuits according to Kirchhoff's rules, the voltages at the load were analytically found $U_{ab} = I_5R_l$ and on the lower shoulder $U_{cb} = I_2p\omega L_a$ antenna inductance, where $\omega = 2\pi f$. The ratio of the source input voltage to the load voltage U_{ab}/U_{cb} is defined as:

$$\frac{U_{ab}}{U_{cb}} = \frac{I_5R_l}{I_2p\omega L_a} = \frac{1}{p},$$

$$U_{ab} = I_5R_l = \frac{I_1p}{X_{La}^{-1} + X_{C1}^{-1} + R_l^{-1}},$$

where X_{La}, X_{C1}, R_l are the inductive, reactive, and active resistances, respectively.

The ratio of the voltage on the antenna to the output voltage of the RF generator is proportional to the ratio of the inductance of the antenna arms at the place where the generator is connected $1/p$. The switching factor p of the upper L_u and lower L_d arms of the antenna is $p = L_d/(L_d + L_u)$.

When inductance L_u appears in the resonant circuit in the upper arm (ca), a phase shift occurs in the U_{ca} and U_{cb} voltages with respect to point c, and the resulting potential difference between (ab) increases [12, 13]. The current consumed from the generator and the current in the load (R_l) is active. At resonant tuning and switching factor p ~1 (low inductance L_u), the voltage U_{ca} and U_{ab} decrease, the phase angle between the vectors U_{cb} and I_1 decreases, the absolute value of the vector I_5 increases, and in the limit the circuit tends to the case presented in Fig. 4.

Diagnostics at the Experimental Stand

A grid probe was used to measure the ion current density. It is attached to the movable vacuum inlet and is located at the output of the plasma emitter. The probe has two electrodes with holes covered by grids and a collector that receives ions, as is shown in Fig. 6. When a voltage is applied between the grid electrodes, a flat plasma boundary is formed, from the surface of which positive ions are drawn out. The area of the probe opening, taking into account the transparency of the grids, is 1.3 mm^2. The collector is at a potential

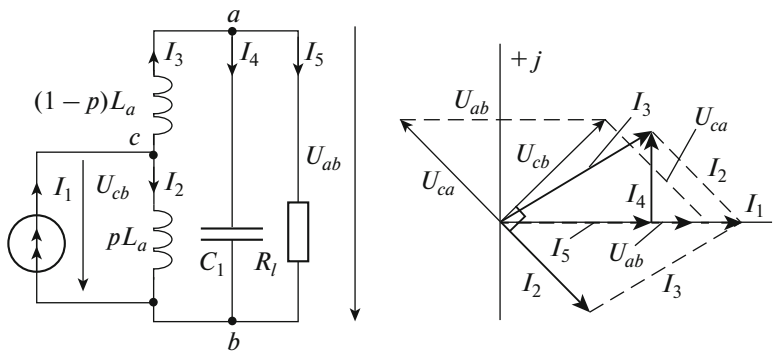

Fig. 5. Connection scheme of the RF generator to the resonant circuit of the RF driver using partial switching. Vector diagrams of currents and voltages for parallel resonance with partial switching are given on the right.

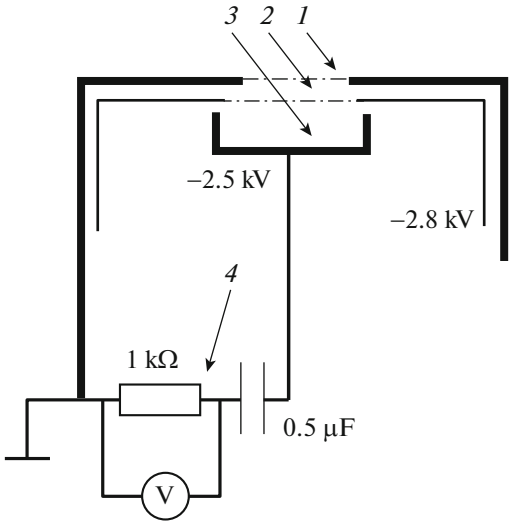

Fig. 6. Scheme of a grid probe for measuring the ion current density: (*1*) external screen with an inlet hole, (*2*) electrode that accelerates ions from the plasma and blocks secondary electrons leaving the collector, (*3*) collector, (*4*) measuring resistance.

of –2.5 kV with respect to the external grid and receives extracted and accelerated ions from the gas-discharge chamber. A grid installed in front of the collector with a potential of –2.8 kV blocks secondary electrons formed on the collector with a potential of –2.5 kV. The probe is located 10 mm further from the level of the connecting flange of the RF driver (position *7* in Fig. 1).

Measurement of the element temperatures and cooling power. The cooling channels for the driver antenna, lower and upper flanges and the ignition unit are connected in parallel using input and output collectors. The protective screen is cooled separately. The flow and water temperature meters are installed on the cooling channels of the RF driver elements and protective screen.

This also made it possible to measure the temperature of the RF driver and its screen through a barium fluoride window in the vacuum chamber immediately after the plasma pulses discharge termination.

3. RESULTS

The following experiments were carried out: the current density on the grid probe was measured with varying RF power in the short pulse mode (50 ms). Since the grid probe is heated by the discharge plasma, the measurements could only be conducted during millisecond pulses. In this case, the gas pressure in the gas-discharge chamber is determined by the ignition valve and is 1–2 Pa.

Thermal loads on the RF driver were studied using calrometric measurements during long pulse operation. In experiments to analyze thermal loads, the duration of the RF discharge pulses was increased to 30 s, and the RF driver configuration with a wide antenna was used. At the initial time, the operation of the RF driver is similar to that at short pulses. When the discharge was ignited, gas was supplied through the second working valve. The pressure in the gas-discharge chamber was set at 0.3–0.6 Pa. Because of the pressure variation in the RF driver during the pulse, the plasma load, with which the RF generator interacts, is also changed.

Measurements of Characteristics of a Driver with a Thin Screen

Ion current density per probe. The results of measuring the ion current density on the probe are shown in Fig. 7. Four antenna configurations were studied in the experiment. The dependences of the plasma ion current density on the RF power have linear trends. The maximum ion current density was 470 mA/cm^2 at an RF power of 64 kW and an antenna amplitude voltage of 10.8 kV with a narrow antenna configuration. The use of ferrites did not provide any advantage over a narrow antenna.

Thermal loads. The results of testing the RF driver in the long-pulse mode showed that the protective screen provides the necessary protection for ceramics: no erosion of ceramics was observed, but some of the molybdenum plates delaminated. Figure 8 shows the supplied RF power and the power load measured during the pulse. In this pulse, an RF power of 32 kW was achieved at an RF voltage at the antenna of 10.2 kV. The characteristic time for establishing the power load was about 15 s. During this time, the power carried by water increases rapidly, after which the growth rate decreases. To estimate the power that goes to induction heating of the driver elements, a pulse was produced with the same voltage, but without igniting the plasma. The RF power consumed in this case corresponds to losses and is 13 kW. Therefore, the power input into the plasma is 19 kW, which corresponds to an estimated efficiency of 19/32 = 59%. It can be also seen from the dependence in Fig. 8 that the power input into the RF driver elements: lower and upper flanges, ignition unit and antenna with and without plasma is almost the same, and the main part of the thermal load goes to the protective screen.

The surface temperatures of the RF driver and screen were measured separately. The results are shown in Figs. 9 and 10. The maximum screen temperature is reached in the middle of the molybdenum plate (*3* in Fig. 10) and is 350°C. The origin of the temperature inhomogeneity is the delamination of molybdenum on some plates. A cooling tube inside the driver can be seen in the picture taken with a thermal imager (*1* in Fig. 10). While it was the orised that the tube could block part of the azimuthal current in plasma

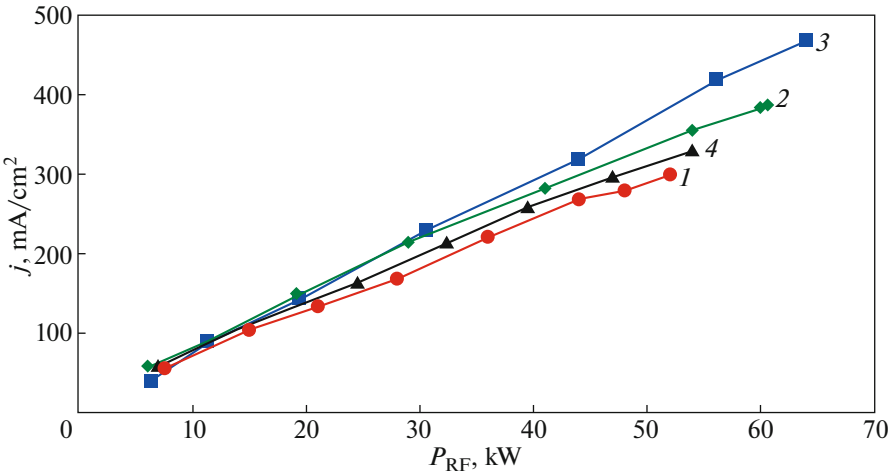

Fig. 7. Current density of positive ions on the probe j depending on the power of the RF generator P_{RF} for an RF driver with a thin screen: (*1*) with a wide antenna shown in Fig. 2b-*1*, (*2*) with a narrow antenna and ferrites shown in Fig. 2b-*3*, (*3*) with a narrow antenna shown in Fig. 2b-*3* without ferrites, (*4*) with a low antenna shown in Fig. 2b-*2*.

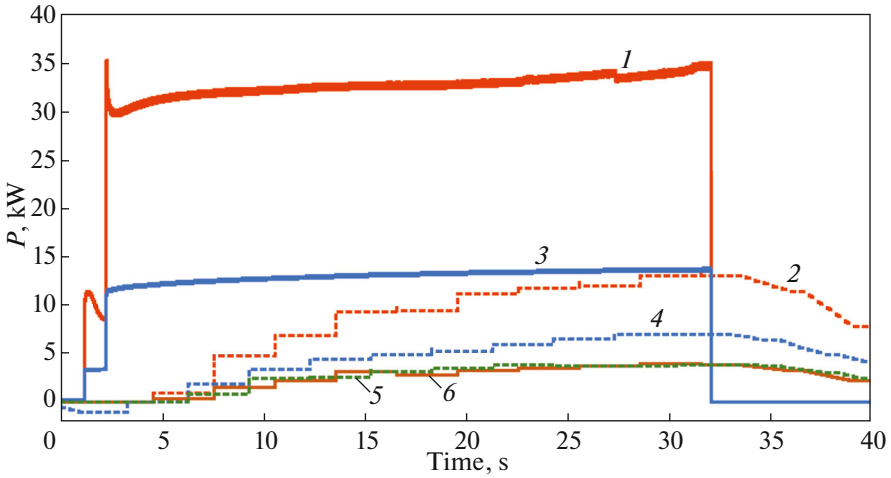

Fig. 8. Oscillograms of the powers supplied from the RF generator ((*1*) with an RF discharge, (*3*) without an RF discharge), and the powers carried away by water from the elements (*2*) from the side surface of the protective screen with an RF discharge, (*4*) from the side surface of the protective screen without an RF discharge, (*5*, *6*) from the antenna, ignition unit, back and front flanges with and without the RF discharge for an RF driver with a thin screen.

and lead to more losses, no significant decreases in efficiency were observed. It can be seen from the outside that the antenna and objects located close to it heat up the most: clamping ring nuts (*3* in Fig. 9), clamping rings and studs. The ceramic temperature was 50°C.

Measurements of Characteristics of a Driver with a Soldered Screen

Ion current density per probe. Experiments similar to those described above were carried out with a soldered screen. A study of the operation of an RF driver with a soldered screen was carried out in [14]. The power dependences of the current density are presented in Fig. 11. The maximum current was obtained with a wide antenna and was 248 mA/cm^2 at an RF power of 55 kW and an antenna voltage of 10.4 kV. The greatest efficiency is achieved in a configuration using ferrites. This may be because the ferrites help concentrate the field within the antenna. At the same time, the inductance of the antenna increases with the addition of the ferrites, and in order to maintain the input power, it is necessary to increase the RF voltage at the antenna. The low antenna configuration has the increased efficiency. This can be explained by the fact

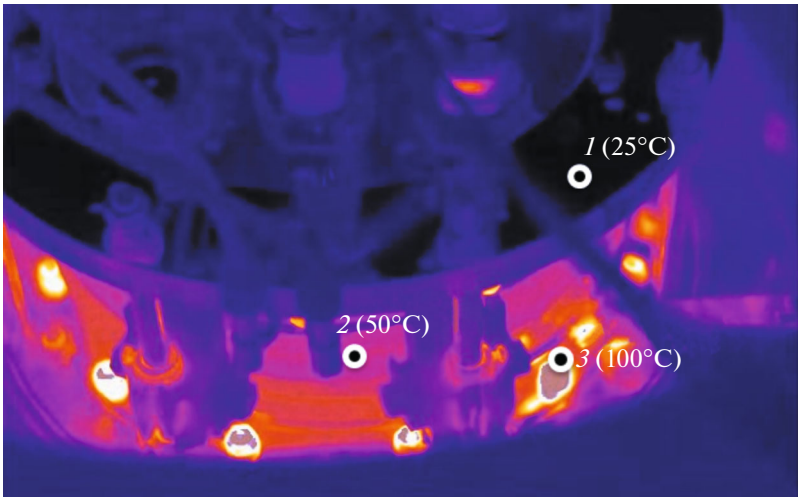

Fig. 9. Photographic image of heating of driver elements with a thin screen at the end of a 33-kW pulse, 30 s (measurements using a thermal imager): (*1*) back flange, (*2*) middle of the ceramic cylinder, (*3*) nut of the lower sealing ring.

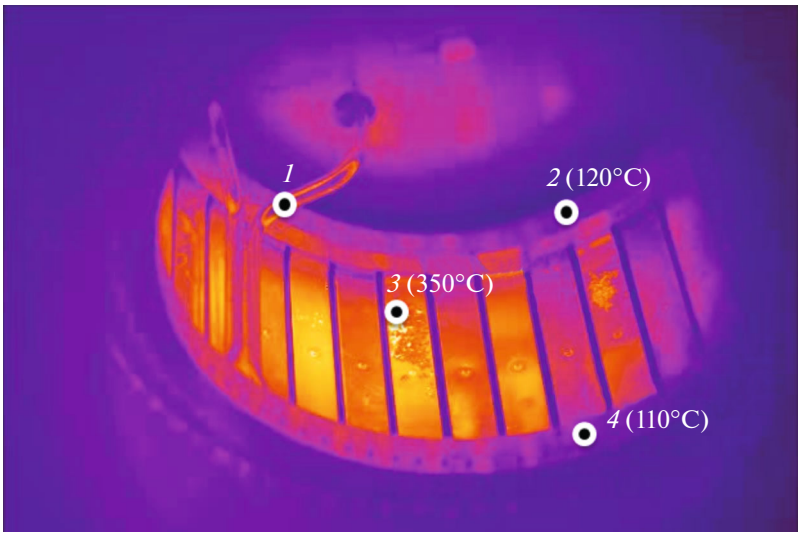

Fig. 10. Photographic image of heating of thin screen elements at the end of a 33-kW pulse, 30 s (measurements using a thermal imager): (*1*) cooling tube of the front ring, (*2*) back cooled ring, (*3*) middle of the plate, (*4*) front cooled ring.

that the antenna in this case is located further from the back wall of the RF driver screen. Because of this, the induced currents in the screen decrease and heat-related losses are reduced.

Thermal loads. The results of testing the driver in the long pulse mode showed that the protective screen provides the necessary protection for ceramics. There were no visible screen deformations, erosion, or dusting of ceramics. Figure 12 shows power loads and the supplied RF power during the pulses. This pulse achieved a power of 26 kW at an antenna voltage of 8.5 kV with a wide antenna configuration. Without plasma, the power was 11 kW, which characterizes the power loss. This corresponds to an estimated efficiency of 58%. Similar to the previous screen, the cooling power of the RF driver elements with and without plasma is almost the same. Power load on the screen sides without plasma is signgificantly larger than it is in the case of the thin screen. This indicates that the losses associated with heating the screen by the RF field have increased compared to a thin screen. The origin is the increase in the surface area of this screen. The characteristic heating time is ~15 s, after which the cooling power reaches the steady-state level. Surface temperatures were not measured for this screen.

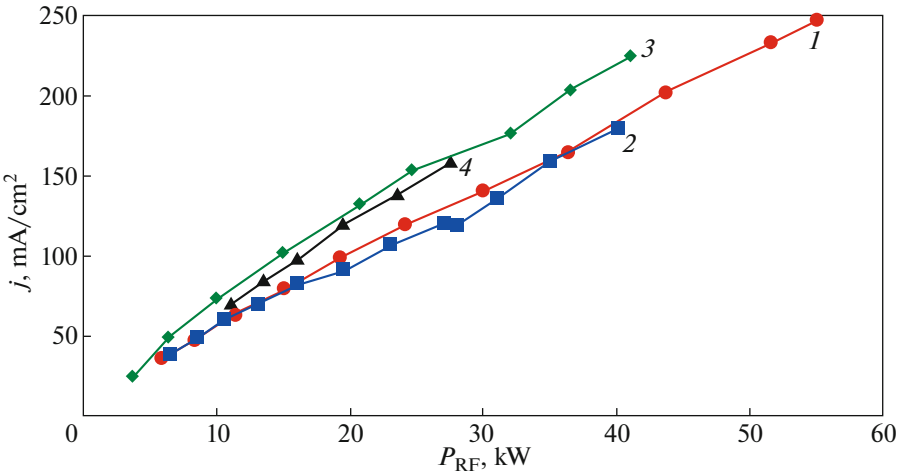

Fig. 11. Current density of positive ions on the probe j depending on the power of the RF generator P_{RF} for an RF driver with a soldered screen: (*1*) with a wide antenna shown in Fig. 2b-*1*, (*2*) with a narrow antenna shown in Fig. 2b-*3* without ferrites, (*3*) with a narrow antenna and ferrites shown in Fig. 2b-*3*, (*4*) with a low antenna shown in Fig. 2b-*2*.

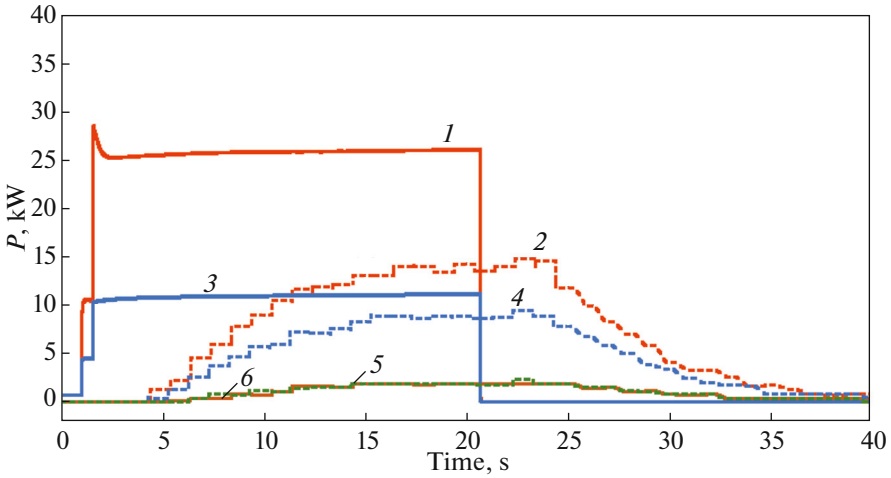

Fig. 12. Oscillograms of the powers supplied from the RF generator ((*1*) with an RF discharge, (*3*) without an RF discharge), and the powers carried away by water from the driver elements: (*2*) from the side surface of the protective screen with an RF discharge, (*4*) from the side surface of the protective screen without the RF discharge, (*5*, *6*) from the antenna, ignition unit, back and front flanges with and without RF discharge for an RF driver with a soldered screen.

Measurements of Characteristics of a Driver with a Screen with Molded Slots

Ion current density per probe. The dependence of the ion current density on the RF power is shown in Fig. 13. The maximum current was achieved with a wide antenna configuration and was 198 mA/cm^2 at a power of 45 kW and an antenna voltage of 10.5 kV. Similar to the soldered screen, the use of ferrites allowed a slight increase in the efficiency; the configuration with a narrow antenna gave the same effect. The field weakly penetrates into the screen. This screen is thicker than others and has a back wall, so it increases the antenna inductance more than others. Because of this, it is necessary to increase the antenna voltage to achieve characteristic RF powers.

Heat loads. The results of testing the generator in the long pulse mode showed that the screen provides the necessary protection for ceramics. No visible screen deformation or ceramic erosion was observed. Figure 14 shows power loads and the supplied RF power during the pulses. This pulse achieved a power of 30 kW at an antenna voltage of 12.8 kV with a wide antenna configuration. At the same time, without plasma, the power loss was 16 kW. This corresponds to an estimated efficiency of 47%. It is clear

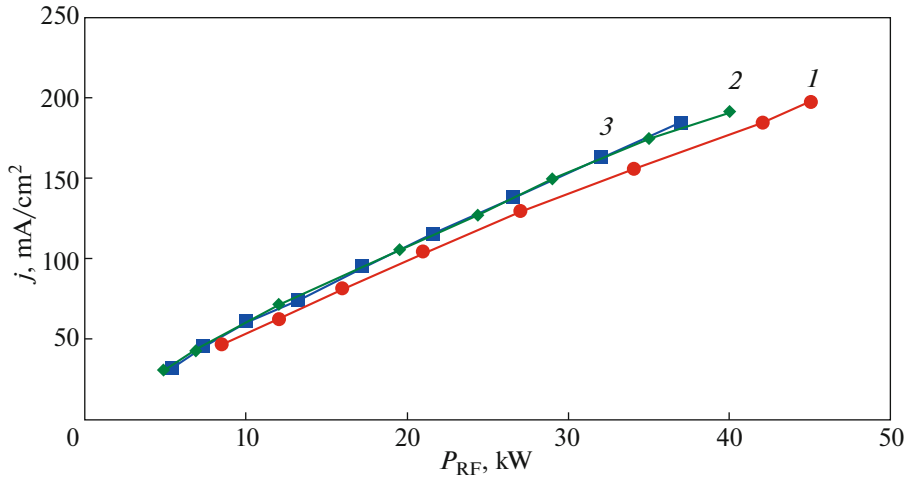

Fig. 13. Current density of positive ions on the probe j depending on the power of the RF generator P_{RF} for an RF driver with a screen with molded slots: (*1*) with a wide antenna shown in Fig. 2b-*1*, (*2*) with a narrow antenna and ferrites shown in Fig. 2b-*3*, (*3*) with a narrow antenna shown in Fig. 2b-*3* without ferrites.

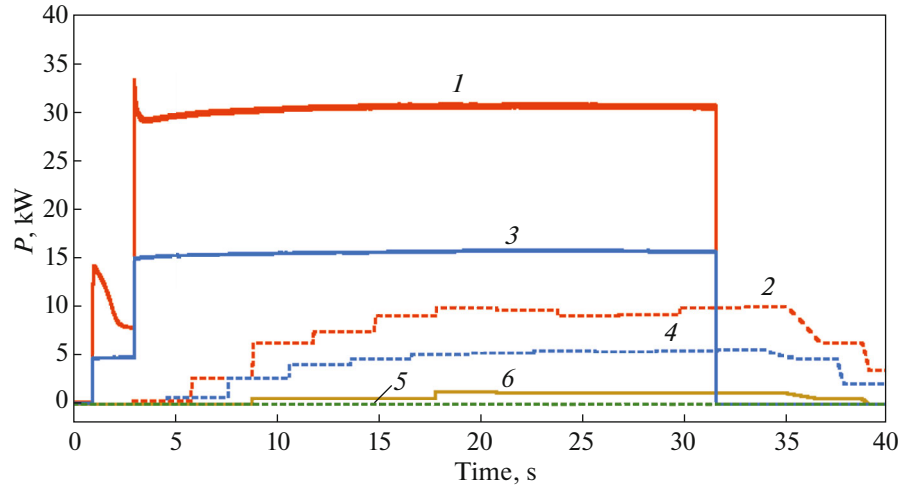

Fig. 14. Oscillograms of powers supplied from the RF generator ((*1*) with an RF discharge, (*3*) without an RF discharge), and the powers carried away by water from the driver elements: (*2*) from the side surface of the protective screen with an RF discharge, (*4*) from the side surface of the protective screen without the RF discharge, (*5*) from the back wall of the protective screen without the RF discharge, (*6*) from the back wall of the protective screen with the RF discharge for an RF driver with a screen with molded slots.

from the dependence that the cooling power of the back wall differs slightly in a pulse with and without plasma. Consequently, the plasma flies weakly onto the back wall of the RF driver, and it is almost not heated by the RF field. The multipole structure of the magnetic field on the back wall of the RF driver significantly reduces the flow of charged particles onto it. The discharge plasma mainly heats the side surface of the protective screen. The characteristic heating time is ~18 s.

Figure 15 shows a photograph obtained using a thermal imager after a 30 s RF pulse with a power of 30 kW. The screen is cooled efficiently, the maximum temperature is 60°C.

4. EFFICIENCY OF USING THE RF POWER

Table 1 shows the characteristics of the drivers described above in the short pulse mode. In the first column, Table 1 shows the screen, the second column shows the maximum RF power deposited into the plasma when using this screen and the voltage on the RF antenna. The third column shows the ion current density per probe, the fourth column shows the effi-

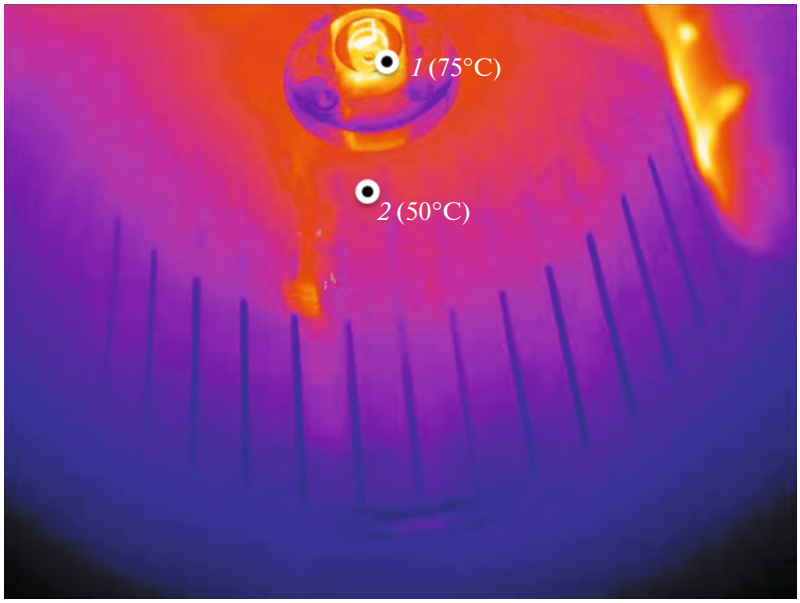

Fig. 15. Photographic image of heating screen elements with molded slots at the end of a 30-kW pulse, 30 s (measurements with a thermal imager): (*1*) ignition unit, (*2*) back wall of the protective screen.

ciency of the RF power deposition in plasma, and the fifth column shows the energy efficiency of the driver.

The maximum efficiency of 59% is achieved with a thin screen. Due to the small thickness of the side wall and the simple structure of the slots, the RF field easily penetrates into the plasma chamber and ionizes the gas. Ions from this region reach the output of the RF driver and form a flow of ions. The energy efficiency of the soldered screen and the screen with molded slots is less than 58 and 47%, respectively. This may be due to the z-shaped structure of the lamellas (see Fig. 3). This structure increases the overall thickness of the side wall.

5. CONCLUSIONS

Three RF driver configurations are developed and experimentally studied. The thin screen provides the plasma preparation with a high current density per probe of 470 mA/cm^2 at an RF power of 64 kW and allows working with pulses with the duration of at least 30 s. The measurements showed that in a pulse lasting 30 s, the temperature of this screen did not reach a steady-state mode, as the cooling power kept increasing. The maximum temperature of the screen lamellas in an RF discharge pulse lasting 30 s was 350°C.

Thus, the RF drivers with a soldered screen and a molded slot screen are suitable for steady-state operation of the ion source. The achieved ion current density for a soldered screen was 248 mA/cm^2 at an RF power of 55 kW. The achieved current density for a screen with molded slots was 198 mA/cm^2 at an RF power of 45 kW. These screens reach the steady-state cooling power in a characteristic time of about 15 s. The efficiency of the power input for an RF driver with a soldered screen is 58%, and that for a screen with molded slots is 47%.

The results of the calorimetric measurements are consistent with the RF power measured at the output of the RF generator for drivers with a soldered screen and a thin screen. Experiments have shown that the power flow to the back wall of the RF driver is signifi-

Table 1. Basic parameters of RF drivers when using various protective screens

Screen	Maximum antenna power/voltage	Current density/current at RF driver output	Efficiency of the power contribution to the plasma	Driver energy efficiency, A/kW	
				on the RF power	on the power input in the plasma
Thin	64 kW/10.8 kV	470 mA/ 105 A	59%	1.64	2.78
Soldered	55 kW/10.4 kV	248 mA/ 57 A	58%	1.04	1.79
With formed slots	45 kW/10.5 kV	198 mA/ 50 A	47%	1.11	2.36

cantly reduced because of the use of a multipole magnetic field.

FUNDING

This work was supported by the Ministry of Science and Higher Education of the Russian Federation. This work was carried out within the Federal project of the Comprehensive program "Development of equipment, technologies and scientific research in the field of use of atomic energy in the Russian Federation."

CONFLICT OF INTEREST

The authors declare that they have no conflicts of interest.

REFERENCES

1. O. Sotnikov, A. Ivanov, Yu. Belchenko, A. Gorbovsky, P. Deichuli, A. Dranichnikov, I. Emelev, V. Kolmogorov, A. Kondakov, A. Sanin, and I. Shikhovtsev, Nucl. Fusion **61**, 116017 (2021).
2. I. Shikhovtsev, G. Abdrashitov, Yu. Belchenko, V. Belov, V. Davydenko, A. Gorbovsky, A. Ivanov, V. Kapitonov, A. Kondakov, V. Mishagin, A. Sanin, O. Sotnikov, and E. Shubin, AIP. Conf. Proc. **2052**, 040016 (2018).
3. I. A. Prokhorov, G. F. Abdrashitov, I. I. Averbukh, V. P. Belov, V. I. Davydenko, A. A. Ivanov, V. A. Kapitonov, V. V. Kolmogorov, A. A. Kondakov, I. V. Shikhovtsev, A. V. Sorokin, and A. A. Tkachev, Fusion Sci. Technol. **63**, 349 (2013).
4. D. Fasel, Y. Andrebe, J. Dubray, A. Karpushov, V. Kolmogorov, B. Marletaz, P. Marmillod, L. Muehle, A. Perez, I. Shikhovtsev, and U. Siravo, Fusion Eng. Des. **123**, 331 (2017).
5. A. Sorokin, V. Belov, V. Davydenko, P. Deichuli, A. Ivanov, A. Podyminogin, I. Shikhovtsev, G. Shulzhenko, N. Stupishin, and M. Tiunov, Rev. Sci. Instrum. **81**, 02B108 (2010).
6. E. Speth, M. Ciric, J. H. Feist, P. Frank, B. Heinemann, W. Kraus, F. Probst, R. Riedl, R. Trainham, O. Vollmer, and R. Wilhelm, Fusion Eng. Des. **46**, 383 (1999).
7. P. McNeely, S. Äkäslompolo, W. Auerweck, Y. Drider, O. P. Ford, D. A. Hartmann, B. Heinemann, S. Heinrich, C. Hopf, R. Kairys, S. Obermayer, R. Riedl, P. Rong, N. Rust, R. Schroeder, et al., Fusion Eng. Des. **161**, 111997 (2020).
8. D. Marcuzzi, P. Agostinetti, M. Dalla Palma, H. D. Falter, B. Heinemann, and R. Riedl, Fusion Eng. Des. **82**, 798 (2007).
9. B. Heinemann, U. Fantz, W. Kraus, L. Schiesko, C. Wimmer, D. Wünderlich, F. Bonomo, M. Fröschle, R. Nocentini, and R. Riedl, New J. Phys. **19**, 015001 (2017).
10. Y. Gu, Y. Xie, J. Wei, Y. Xu, J. Li, C. Jiang, L. Liang, Y. Xie, and C. Hu, Rev Sci. Instrum. **90**, 113315 (2019).
11. P. C. Sen, *Principles of Electric Machines and Power Electronics* (Wiley, New York, 1997).
12. G. I. Atabekov, *Fundamentals of Circuit Theory* (Lan', St. Petersburg, 2009) [in Russian].
13. I. S. Gonorovskii, *Radio Engineering Circuits and Signals* (Sov. Radio, Moscow, 1963) [in Russian].
14. V. A. Vointsev, D. Yu. Gavrisenko, A. A. Kondakov, O. Z. Sotnikov, and R. A. Finashin, Sib. Fiz. Zh. **17** (3), 5 (2022).

Translated L. Mosina